Journal of the Korean Physical Society, Vol. 68, No. 12, June 2016, pp. 1403∼1408

Frequency-dependence of the Switching Voltage in Electronic Switching of Pt-dispersed SiO_2 Thin Films

Byung Joon Choi*
Department of Materials Science and Engineering, Seoul National University of Science and Engineering, Seoul 01811, Korea

I-Wei Chen
Department of Materials Science and Engineering, University of Pennsylvania, Philadelphia, Pennsylvania 19104, USA

(Received 9 September 2015)

The switching time-voltage dependence of electronic resistive switching was studied for understanding the switching dynamics in Pt-dispersed SiO_2 thin film devices. Trapezoidal voltage pulses with opposite polarities were consecutively introduced and thereby transient on-switching and off-switching were examined. A prior on-switching voltage determines the off-switching voltage regardless of the sweeping rate of the pulse for the prior on-switching. However, the off-switching voltage was sensitive to the sweeping rate of the subsequent pulses for off-switching. The frequency-dependent impedance of both the device and the surrounding circuit element are thought to result in the variation of the off-switching voltage; otherwise, the switching voltage is independent of time.

PACS numbers: 71.30.+h, 72.80.Tm, 73.50.Mx
Keywords: Metal-insulator transition, Composite materials, Charge transport
DOI: 10.3938/jkps.68.1403

I. INTRODUCTION

Resistive random access memories (ReRAMs) have attracted considerable interest on account of their simple structure, ultrafast write/read access, and high write/erase cycle number. Resistive switching can originate from various physical or physicochemical phenomena such as ionic motion, electronic trapping and phase change [1–3]. The underlying switching dynamics may help clarify the switching mechanisms. Practically, the switching dynamics can also enable circuit designers to predict the switching behavior of the device under an arbitrary voltage and current bias and to investigate the fundamental principles underneath [4]. Ionic motion-based resistive switching shows strongly nonlinear switching dynamics; thus the switching speed depends strongly on the applied voltage or current [4–7]. For example, a 10-fold (0.5 V to 5 V) increase of voltage could result in a 9 orders of magnitude (100 s to 100 ns) decrease on the switching time [6]. Such a strong nonlinearity can be rationalized by the enhanced ionic drift under an extremely high field and temperature within a range of a few nm range [6,7]. On the other hand, such a thermo-chemical dependence of the switching speed may cause variations in the switching parameters (voltage and resistance) from device to device because the environment of an individual memory cell can vary greatly in highly-integrated memory chips [8,9].

Recently, purely electronic switching phenomena in systems of random materials have been reported, which were inspired by Anderson's localization theory [10–13]. These thin-film devices consist of a mixture of metal atoms and metal nanoparticles dispersed in a dielectric thin film or an atomic mixture of conducting and insulating perovskite unit cells in single-crystal-like films, sandwiched between a bottom and a top electrode [10–15]. An extremely uniform and reliable bipolar resistance switching behavior has been obtained with a fast operation speed (100 ps), a large R_{off}/R_{on} ratio ($>$ 100), a long retention ($>$ 10 years) and low programming/reading voltages [14, 15]. Another merit of electronic switching may lie in its much simpler switching dynamics relying on the intrinsic electronic ballistic, collisional or tunneling motion, or the circuit delay characteristics, rather than on the extrinsic environment, such as elevated temperature or neighboring memory cell, which may influence ionic motion [10, 13]. In this study, frequency-dependent resistive switching was investigated, and in this paper, the influence of the circuit's delay characteristics on the switching dynamics is discussed.

*E-mail: bjchoi@seoultech.ac.kr; Fax: +82-2-973-6657

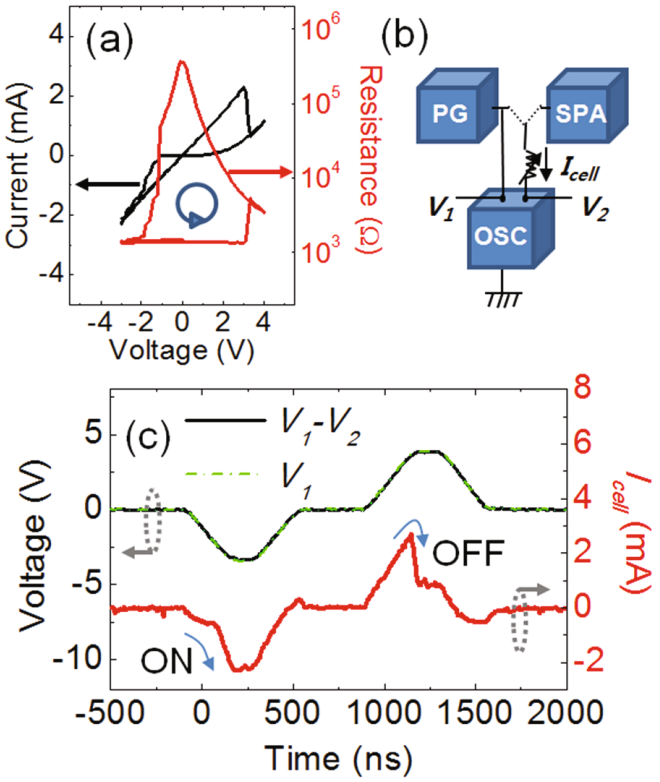

Fig. 1. (Color online) (a) Typical current − voltage (I-V) and resistance − voltage (R-V) curves of a 20-nm-thick SiO_2:0.27Pt thin film with metal electrodes. (b) Schematic diagram of the electrical measurement system. (c) Pulse waveforms of the voltage (V_{cell} and V_{app})- and the current (I_{cell})-related sequential on- and off-switching acquired from the oscilloscope.

II. EXPERIMENTS AND DISCUSSION

The test cell was fabricated on thermally-grown 200-nm-thick SiO_2 formed on a Si substrate. A 30-nm-thick Mo bottom electrode was deposited by DC magnetron sputtering, and a 20-nm-thick Pt dispersed SiO_2 thin film was co-deposited by using RF magnetron sputtering with Mo, SiO_2 and Pt targets, respectively. A Pt top electrode was deposited by sputtering and was lithographically patterned (20 × 20 to 80 × 80 μm^2 in area for top electrode probing). A 4-nm-thick Al_2O_3 capping layer was grown by using atomic layer deposition (ALD) to prevent moisture-mediated degradation of the memory switching [16,17]. The static (dc) current - voltage (I-V) and resistance - voltage (R-V) characteristics were examined using a semiconductor parameter analyzer (SPA, Keithley 237). The dynamic on- and off-switching characteristics were tested by using a pulse measurement system consisting of an Agilent 81104A pulse generator (PG) and an HP Infinium 54825A oscilloscope (OSC). A bias voltage was applied to the top Pt electrode while the bottom contact was grounded.

Typical dc I-V and R-V curves of the cell with 20 nm of SiO_2:0.27Pt are plotted in Fig. 1(a). The figure shows bipolar-type resistive switching, *i.e.*, switching from a low resistance state (LRS) to a high resistance state (HRS) at a positive bias and then reversing at a negative bias. Trapping (detrapping) of electrons to atomically-dispersed Pt atoms or to the Pt/SiO_2 interface is considered to be responsible for the off- (on-) switching [11].

Figure 1(b) shows a schematic diagram of the pulsed signal measurement system. The pulse generator consists of a current source and an internal resistor, which can provide a programmed voltage by splitting the current into the internal resistor and the external resistor, the latter including the resistive switching device and the internal resistance of the oscilloscope. The voltage across the device (V_{cell}) can be acquired by subtracting the voltage across the series resistor (V_2) from the one across the parallel resistor of the oscilloscope (V_1). The current passing through the device (I_{cell}) can be considered to be the same as the one monitored by the series resistor of the oscilloscope [18–20].

To determine the switching voltage and the time that the resistance changes from the transient pulse waveform, we applied a trapezoidal shaped voltage pulse with a voltage sweeping rate (υ_{sweep}). Figure 1(c) shows the waveforms of the voltage ($V_{cell} = V_1 - V_2$) and the current (I_{cell}) acquired from the separate channels of the oscilloscope in the upper and the lower panels, respectively. A negative bias pulse for the transition from the HRS to the LRS (on-switching) was followed by a positive pulse for the opposite transition (off-switching).

To validate this protocol, we examined the response of off-switching when the LRS was set by the different on-switching voltage ($V_{cell,on}$) and lead time, t_{lead} ($t_{lead} = V_{cell}/2\upsilon_{sweep}$) used. Figure 2(a) show the pulse waveforms of V_{cell} and I_{cell} with value of t_{lead} from 200 ns (purple curve) to 500 ns (orange curve) for the prior on-switching. After that, the same magnitude of the positive voltage pulse was applied for the off-switching. Both waveforms showed an abrupt current drop at the same time and thus the same voltage level. Figure 2(a) also shows that decreasing $V_{cell,on}$ from −3.5 to −2.5 V (purple vs. green curve) gives rise to a shortened switching time and a decreased $V_{cell,off}$. Figure 2(b) show the $V_{cell,off}$ as a function of $V_{cell,on}$ along with the lead time, confirming that $V_{cell,off}$ was indeed, proportional to $V_{cell,on}$. This means the off-switching voltage is determined by amplitude of the voltage that enforced the prior on-switching, regardless of the value of t_{lead} of on-switching. Such a characteristic-that the off-switching voltage is determined by the on-switching voltage-during pulse switching is entirely consistent with the previously-reported characteristic in dc switching [10,12].

Next, we examined off-switching for various value of the sweep rate (υ_{sweep}) while keeping the prior on-switching pulse condition fixed ($V_{cell,on} = -3.5$ V, t_{lead} = 500 ns). The pulse height for off-switching was fixed at +4 V. Figure 3(a) presents the waveforms of V_{cell} and

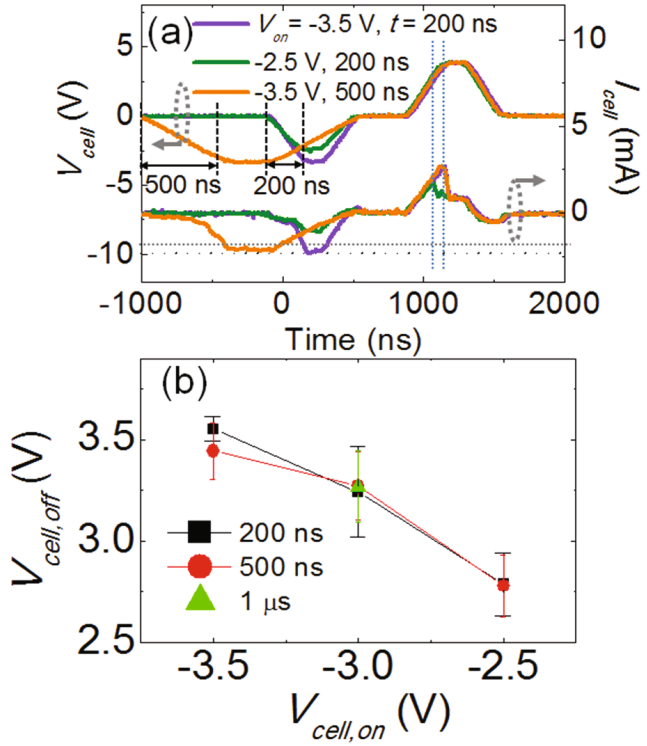

Fig. 2. (Color online) (a) Pulse waveforms of V_{cell} and I_{cell} with different t_{lead} (200 and 500 ns) and $V_{cell,on}$ (−2.5 and −3.5 V) for the prior on-switching and following off-switching. (b) Variation of $V_{cell,off}$ as a function of $V_{cell,on}$, where $V_{cell,off}$ depended linearly on $V_{cell,on}$ irrespective of t_{lead} for on-switching.

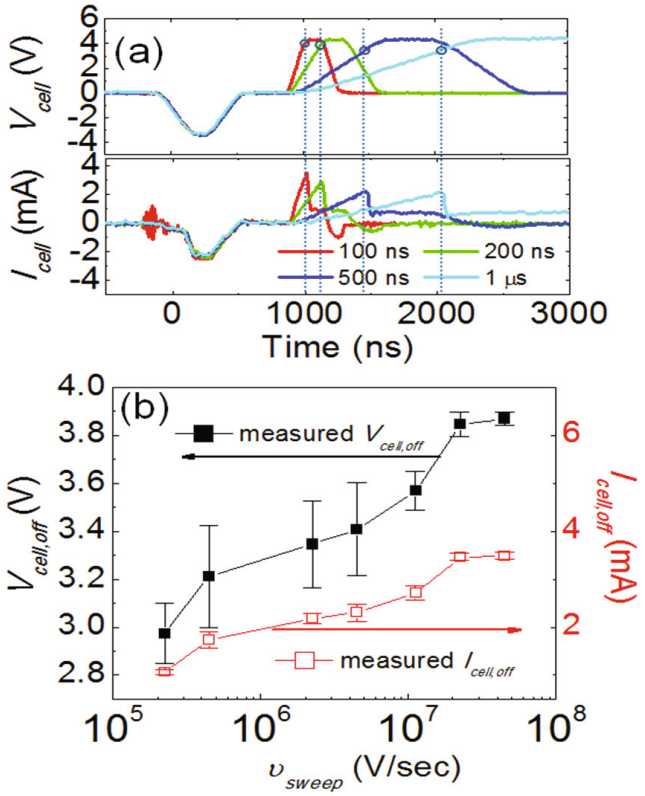

Fig. 3. (Color online) (a) Pulse waveforms of V_{cell} and I_{cell} for various of sweep rates (υ_{sweep}) from (t_{lead} = 1 μs) to (t_{lead} = 100 ns) for off-switching while fixing prior on-switching pulse condition ($V_{cell,on}$ = −3.5 V, t_{lead} = 500 ns). (b) $V_{cell,off}$ (left) and $I_{cell,off}$ (right) as functions of υ_{sweep}.

I_{cell} with varying υ_{sweep} from 2×10^6 (t_{lead} = 1 μs) to 2×10^7 V/sec (t_{lead} = 100 ns). With increasing υ_{sweep}, off-switching is noted to have occurred at a higher current and voltage level, as shown in Fig. 3(b), in which both $V_{cell,off}$ and $I_{cell,off}$ monotonically increased with increasing υ_{sweep}. Thus, at different υ_{sweep}, $V_{cell,off}$ is not just determined by the magnitude of $V_{cell,on}$ [10,15]. These results can be explained from the viewpoint of the circuit response as discussed below.

First, the equivalent circuit of the memory device shown in Fig. 4(a) is considered as a series combination of the parallel resistor and capacitor of the memory element (R_m and C_m), the parallel resistor and capacitor of the interface element (R_i and C_i), and the resistor of the electrode (R_e). R_m and C_m of the memory element are responsible for the resistive switching, where the generation of conducting paths largely modulates R_m whereas C_m comes from the background dielectric materials. R_e mostly comes from the resistance of the Mo bottom electrode; particularly in this device, ∼350 Ω was measured [10]. R_i and C_i are considered to originate from the interface surrounding the electrode, such as the interfacial layer between the Mo electrode and the dielectric materials [16,17]. The combination of parallel resistors and capacitors could be simplified to the impedance of the test device, Z_{cell}.

Second, the equivalent circuit of the measurement system, which is the same as in Fig. 1(b), is shown in Fig. 4(b). All impedances from the measurement instruments, for instance, the internal resistor, of Z_{PG} and internal resistors of the oscilloscope (Z_1 and Z_2) can be expressed as a simple resistor due to their negligible parasitic capacitances [19]. Now, we can express I_{cell} and V_{cell} in terms of the impedance of the circuit elements and applied voltage ($V_{app} = V_1$) as

$$V_1 = V_{cell} + I_{cell} Z_2, \tag{1}$$

$$I_{PG} = \frac{V_1}{Z_{PG}} + \frac{V_1}{Z_1} + \frac{V_{cell}}{Z_{cell}}. \tag{2}$$

From Eqs. (1) and (2), we can obtain the following relationships between V_{cell}, I_{cell} and Z_{cell}:

$$V_{cell} = I_{PG} \frac{Z_p}{Z_{cell} + Z_2 + Z_p} Z_{cell} = I_{cell} Z_{cell}, \tag{3}$$

$$I_{cell} = I_{PG} \frac{Z_p}{Z_{cell} + Z_2 + Z_p}. \tag{4}$$

Here PG provides a current, which is to generate a voltage difference, to the external impedance (50 Ω declared) with an internal resistor (Z_{PG} = 50 Ω); thus,

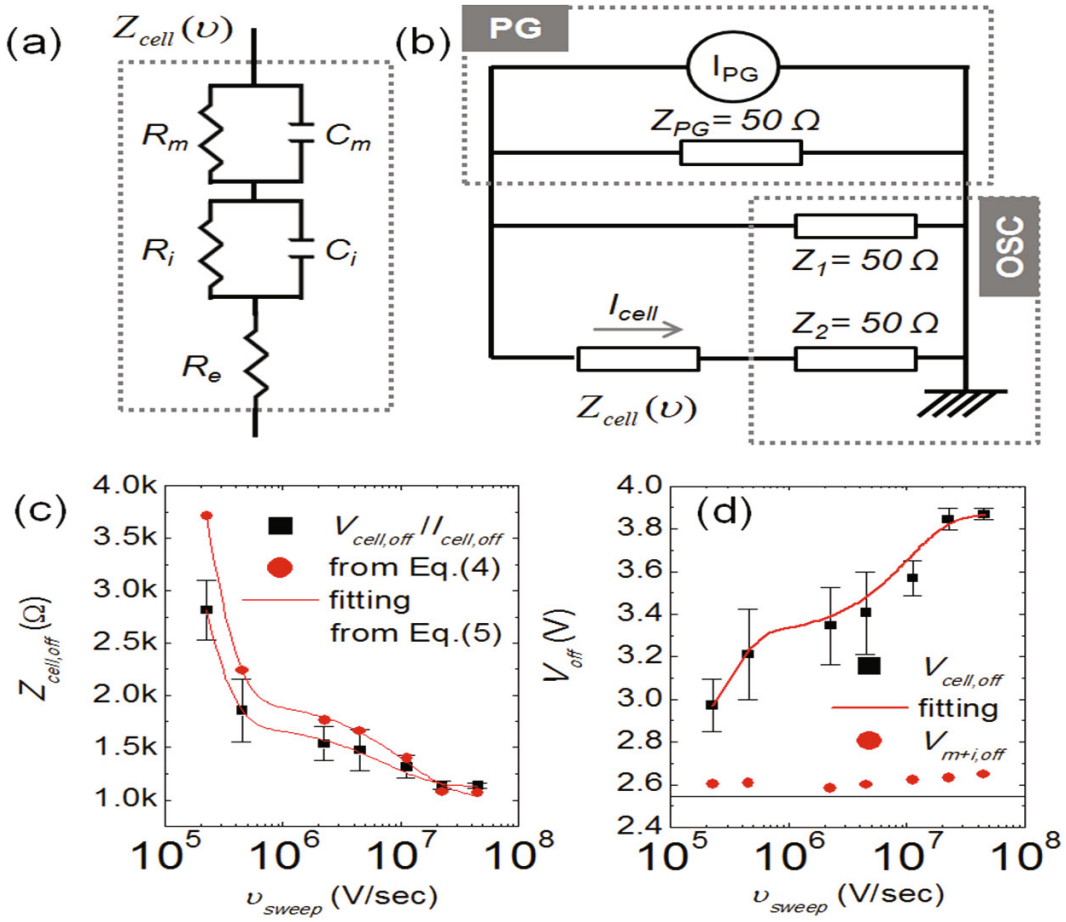

Fig. 4. (Color online) (a) The equivalent circuit of the memory device considered as the series combination of the parallel resistor and capacitor of the memory element (R_m and C_m), the parallel resistor and capacitor of the interface element (R_i and C_i), and resistor of the electrode (R_e). (b) The equivalent circuit of the pulse measurement system. (c) $Z_{cell,off}$ calculated from the measured $V_{cell,off}$ and $I_{cell,off}$ (squares) and calculated from Eq. (4) (circles). The fitting results were obtained by using Eq. (5). (d) $V_{cell,off}$ fitted with $Z_{cell,off}$ as a function of υ_{sweep}, where the threshold voltage for off-switching, $V_{th} \sim 2.55 \pm 0.02$ V (straight line below), was comparable to $V_{m+i,off}$ (red circles) estimated from $I_{cell,off} \times (Z_{cell,off} - R_e)$.

Table 1. Fitting parameters for Eq. (5) for satisfying the frequency-dependent impedance of the memory cell, $Z_{cell}(\upsilon)$.

	Z_0 (Ω)	A_1 (Ω)	τ_1 (V/sec.)	A_2 (Ω)	τ_2 (V/sec.)
$V_{cell,off}/I_{cell,off}$	1130.5	7423.6	1.18020×10^5	600.03	7.2736×10^6
From Eq. (4)	1024.8	9866.3	1.31100×10^5	933.50	1.10612×10^7

I_{PG} can be simply calculated (*i.e.* $I_{PG} = V_1/25$). Z_p consists of parallel Z_{PG} (50 Ω) and Z_1 (50 Ω) and is thus, 25 Ω. Z_2 is also fixed to 50 Ω. Accordingly, Z_{cell} can be effectively estimated by using the V_{cell} and the I_{cell} measured by the instrument. Figure 4(c) shows $Z_{cell,off}$ (square) acquired from the measured $V_{cell,off}$ and $I_{cell,off}$ (shown in Fig. 3(b)) as functions of υ_{sweep}. It also shows $Z_{cell,off}$ (circle) directly acquired from I_{cell} according to Eq. (4), where both values decrease abruptly with increasing υ_{sweep} and then saturate. Such a frequency-dependent variation of the impedance can be understood from the relaxation or recovery transient upon the sudden application and removal of an external stress, herein the voltage pulse with the high-frequency modulating [21].

The frequency-dependent impedance of the device, $Z_{cell,off}$ (υ_{sweep}), namely, Z_{cell} (υ), can be successfully fitted by using the equation for double exponential decay as shown in Fig. 4(c):

$$Z(\upsilon) = Z_0 + A_1 \exp(-\upsilon/\tau_1) + A_2 \exp(-\upsilon/\tau_2), \quad (5)$$

where τ_1 and τ_2 can be considered as the inverses of the

time constants ($1/RC$) in the parallel RC circuits of the memory element (R_m and C_m) and the interface element (R_i and C_i), respectively. The fitting results for both values of $Z_{cell,off}$ are presented in Table 1. The slower or smaller τ_1 ($\sim 10^5$ V/sec) originated from the capacitive element of the interface that is reasonable because it is responsible for charging and discharging a wide area of the device and its vicinity whereas the faster or larger τ_2 ($\sim 10^7$ V/sec.) come from the capacitive element of the memory in which the transient times of switching follow a dispersion relationship with the device area at high υ_{sweep} (data not shown).

Now, Z_{cell} (υ) can be used for representing $V_{cell,off}$ (υ) by reconstructing Eq. (3):

$$\begin{aligned} V_{cell}(\upsilon) &= I_{cell}Z_{cell} = I_{cell}\{(Z_m + Z_i) + R_e\} \\ &= V_{th}\left(1 + \frac{R_e}{Z_{cell}(\upsilon) - R_e}\right), \end{aligned} \quad (6)$$

where V_{th} is the threshold voltage for the off-switching solely applied to the memory and interface, which can be calculated from $I_{cell} \times (Z_m + Z_i)$. As shown in Fig. 4(d), Eq. (6), with a single best-fit V_{th} of 2.55 ± 0.02 V (noted as the straight line at the bottom), can be successfully used to fit the data and obtain $V_{cell,off}$ (same as Fig. 3(b)). Note that a single value of V_{th} means the true voltage for the off-switching is identical irrespective of υ_{sweep}, which is expected for an electronic switching nanometallic memory. The threshold voltage for off-switching could be estimated from $I_{cell,off} \times (Z_{cell,off} - R_e)$ noted as $V_{m+i,off}$ (red circles), which was, indeed, comparable to the fitted value (straight line) and almost insensitive to υ_{sweep} in Fig. 4(d).

Previous work on voltage pulse-induced switching of nanometallic memory revealed that the switching voltages for both on- and off-switching were invariant to the pulse width, temperature or device area [11,12,15]. The major difference between this work and the previous work is how to apply the time-varying voltage pulse in a different manner. When pulse widths were varied from 100 ns to several ms for varying the switching time in the previous work, t_{lead} was set to 2 ns; thereby, υ_{sweep} was actually high enough, such as $\sim 10^8$ V/sec. Therefore, Z_{cell} (υ) had already decreased and saturated to a small value. On the other hand, when υ_{sweep} was varied from 10^5 to 5×10^7 V/sec as in this work, then Z_{cell} (υ) showed a υ_{sweep} dependence, which resulted in the weak time-dependent switching behavior. Note that a typical memristor or ionic switching memory demands at least twice the voltage to achieve ∼10 times R_{off}/R_{on} switching in the pulse duration range from 100 ns to 1 ms [6]. Therefore, the nonlinear switching dynamics of a memristor can explain neither the pulse-width-independent nor weak υ_{sweep}-dependent switching voltage, which again implies that an electronic switching mechanism dominates the nanometallic memory.

III. CONCLUSION

In conclusion, an ReRAM cell was fabricated using a 20-nm of SiO_2:0.27Pt film between the Mo bottom and the Pt top electrodes. When a trapezoidal-shaped voltage pulse was introduced, the off-switching parameters were determined by the previous on-switching voltage. Meanwhile, $V_{cell,off}$ also depended on the υ_{sweep} of the voltage pulse for off-switching: a higher υ_{sweep} lead to a higher $V_{cell,off}$. This time dependence of $V_{cell,off}$ was caused by the circuit distortion of the excitation voltage, where left a smaller voltage for the switching device (cell) than the nominal applied voltage. From the view point of the circuit, the impedance of the cell, Z_{cell} (υ), can be considered as a combination of the parallel RC circuits of the memory, the interface and the electrode. When υ_{sweep} is increased, Z_{cell} (υ) is decreased; thus, the cells supports a smaller voltage, which, in turn, demands a higher $V_{cell,off}$ to reach the same threshold voltage at the cell for triggering the off-switching of the memory.

ACKNOWLEDGMENTS

This study was supported by Basic Science Research Program through the National Research Foundation of Korea (NRF) funded by the Ministry of Education (NRF-2014R1A1A2054597). IWC was supported by a U.S. National Science Foundation Grant (No. DMR-1409114).

REFERENCES

[1] G. W. Burr, B. N. Kurdi, J. C. Scott, C. H. Lam, K. Gopalakrishnan and R. S. Shenoy, IBM J. Res. Dev. **52**, 449 (2008).
[2] R. Waser, R. Dittmann, G. Staikov and K. Szot, Adv. Mater. **21**, 2632 (2009).
[3] K. Terabe, T. Hasegawa, T. Nakayama and M. Aono, Nat. **433**, 47 (2005).
[4] M. D. Pickett, D. B. Strukov, J. L. Borghetti, J. J. Yang, G. S. Snider, D. R. Stewart and R. S. Williams, J. Appl. Phys. **106**, 074508 (2009).
[5] D. Ielmini, C. Cagli and F. Nardi, Appl. Phys. Lett. **94**, 063511 (2009).
[6] S. Menzel, M. Waters, A. Marchewka, U. Böttger, R. Dittmann and R. Waser, Adv. Func. Mater. **21**, 4487 (2011).
[7] D. B. Strukov and R. S. Williams, Appl. Phys. A Mater. Sci. Proc. **94**, 515 (2008).
[8] D. S. Jeong, R. Thomas, R. S. Katiyar, J. F. Scott, H. Kohlstedt, A. Petraru and C. S. Hwang, Rep. Prog. Phys. **75**, 076502 (2012).
[9] J. J. Yang, D. B. Strukov and D. R. Stewart, Nat. Nanotechnol. **8**, 13 (2013).
[10] A. B. K. Chen, B. J. Choi, X. Yang and I-W. Chen, Adv. Func. Mater. **22**, 546 (2012).

[11] A. B. K. Chen, S. G. Kim, Y. Wang, W.-S. Tung and I-W. Chen, Nat. Nanotechnol. **6**, 237 (2011).
[12] B. J. Choi, A. B. K. Chen, X. Yang and I.-W. Chen, Adv. Mater. **23**, 3847 (2011).
[13] X. Yang, A. B. K. Chen, B. J. Choi and I.-W. Chen, Appl. Phys. Lett. **102**, 043502 (2013).
[14] B. J. Choi *et al.*, Nano Lett. **13**, 3213 (2013).
[15] X. Yang, I. Tudosa, B. J. Choi, A. B. K. Chen and I.-W. Chen, Nano Lett. **14**, 5058 (2014).
[16] X. Yang, B. J. Choi, A. B. K. Chen and I.-W. Chen, ACS Nano **7**, 2302 (2013).
[17] B. J. Choi and I.-W. Chen, Appl. Phys. A Mater. Sci. Proc. **112**, 235 (2013).
[18] B. J. Choi, S. Choi, K. M. Kim, Y. C. Shin, C. S. Hwang, S. Y. Hwang, S. S. Cho, S. Park and S. K. Hong, Appl. Phys. Lett. **89**, 012906 (2006).
[19] D. S. Jeong, H. Lim, G.-H. Park, C. S. Hwang, S. Lee and B. Cheong, J. Appl. Phys. **111**, 102807 (2012).
[20] S. J. Song, K. M. Kim, G. H. Kim, M. H. Lee, J. Y. Seok, R. Jung and C. S. Hwang, Appl. Phys. Lett. **96**, 112904 (2010).
[21] A. K. Jonscher, J. Phys. D: Appl. Phys. **32**, R57 (1999).